Wave Composition, Propagation, and Polarization of Magnetohydrodynamic Turbulence within 0.3 au as Observed by Parker Solar Probe

Xingyu Zhu[1], Jiansen He[1], Daniel Verscharen[2,3], Die Duan[1], and Stuart D. Bale[4,5,6,7]

[1] School of Earth and Space Sciences, Peking University, No. 5 Yiheyuan Road, Haidian District, Beijing, 100871, People's Republic of China; jshept@pku.edu.cn
[2] Mullard Space Science Laboratory, University College London, Dorking RH5 6NT, UK
[3] Space Science Center, University of New Hampshire, Durham NH 03824, USA
[4] Physics Department, University of California, Berkeley, CA 94720-7300, USA
[5] Space Sciences Laboratory, University of California, Berkeley, CA 94720-7450, USA
[6] The Blackett Laboratory, Imperial College London, London SW7 2AZ, UK
[7] School of Physics and Astronomy, Queen Mary University of London, London E1 4NS, UK

Abstract

Turbulence, a ubiquitous phenomenon in interplanetary space, is crucial for the energy conversion of space plasma at multiple scales. This work focuses on the propagation, polarization, and wave composition properties of the solar wind turbulence within 0.3 au, and its variation with heliocentric distance at magnetohydrodynamic scales (from 10 s to 1000 s in the spacecraft frame). We present the probability density function of propagation wavevectors (PDF $(k_{\parallel}, k_{\perp})$) for solar wind turbulence within 0.3 au for the first time: (1) wavevectors cluster quasi-(anti-)parallel to the local background magnetic field for $kd_i < 0.02$, where d_i is the ion inertial length; (2) wavevectors shift to quasi-perpendicular directions for $kd_i > 0.02$. Based on our wave composition diagnosis, we find that: the outward/anti-sunward Alfvén mode dominates over the whole range of scales and distances, the spectral energy density fraction of the inward/sunward fast mode decreases with distance, and the fractional energy densities of the inward and outward slow mode increase with distance. The outward fast mode and inward Alfvén mode represent minority populations throughout the explored range of distances and scales. On average, the degree of anisotropy of the magnetic fluctuations defined with respect to the minimum variation direction decreases with increasing scale, with no trend in distance at any scale. Our results provide comprehensive insight into the scenario of transport and transfer of the solar wind fluctuations/turbulence in the inner heliosphere.

Unified Astronomy Thesaurus concepts: Heliosphere (711); Alfven waves (23); Slow solar wind (1873); Interplanetary turbulence (830)

1. Introduction

The solar corona dynamically expands into interplanetary space in the form of the continuous solar wind (Parker 1958; Coleman 1966), the birth and the acceleration mechanism of which are still not well understood (Tu et al. 2005; He et al. 2007; Cranmer & Winebarger 2019). The solar wind flowing into interplanetary space carries information about its source region, and involves diversified nonlinear physical processes (Tu & Marsch 1995; Bruno & Carbone 2013). It is essential to investigate the nature of near-Sun fluctuations in order to analyze and understand these nonlinear physical processes as well as the heating and acceleration mechanisms of the solar wind.

The statistical properties of the solar wind generally vary with speed, location, and type of source region and heliocentric distance (Bavassano et al. 1982; Tu et al. 1989; He et al. 2013; Matteini et al. 2014; Horbury et al. 2018; Stansby & Horbury 2018; Perrone et al. 2019; Wang et al. 2019; Bandyopadhyay et al. 2020; Chen et al. 2020; Chhiber et al. 2020; Duan et al. 2020; Qudsi et al. 2020). Tu et al. (1989) contrast the properties of magnetohydrodynamic (MHD) turbulence between high-speed and low-speed solar wind at 0.3 au using the spectra of Elsässer variables, cross helicity, residual energy, Alfvén ratio, and Elsässer ratio. They consider that, compared to the high-speed wind, the turbulence evolves in an advanced state in slow wind, due to the longer expansion time. The z^+ and z^- are close to a balanced state with an approximate -1.67 spectral index. The mode composition therein is dominated by the Alfvén

mode and slow mode in the incompressible limit (Dobrowolny et al. 1980). Bavassano et al. (1982) studied the variation of the nature of the fluctuations with heliocentric distance and scale in the trailing edge of a stream interaction region. The anisotropy defined with respect to the direction corresponding to the minimum eigenvalue decreases as the heliocentric distance increases and the scale decreases. The magnetic field closer to the Sun is more compressed. However, Chen et al. (2020) reported the evolution of solar wind turbulence from 0.17 au to 1 au, recently, and find at 0.17 au that: (1) the spectra of magnetic field, velocity, and Elsässer variables present a $-3/2$ slope at MHD scales; (2) the magnetic field is less compressed; and (3) the outward-propagating Alfvén waves are more dominant than at 1 au. Fast solar wind is characterized by highly Alfvénic fluctuations, although a new type of Alfvénic slow solar wind, possibly coming from quiet-Sun regions or coronal-hole boundaries, has been reported at distances from 0.3 au to 1 au (D'Amicis & Bruno 2015; Wang et al. 2019; Parashar et al. 2020; Perrone et al. 2020). It is of interest to study this kind of solar wind, on account of its distinct properties, which differ from the classical slow solar wind.

Even if we relax the assumption of a pure superposition of linear waves, nonlinear turbulent fluctuations still retain certain polarization and correlation properties of linear modes (Tu & Marsch 1995). When we use the term "wave," we refer to the mode composition of the fluctuations within this wave-turbulence paradigm. The composition of wave modes in the solar wind near 1 au has been extensively studied and
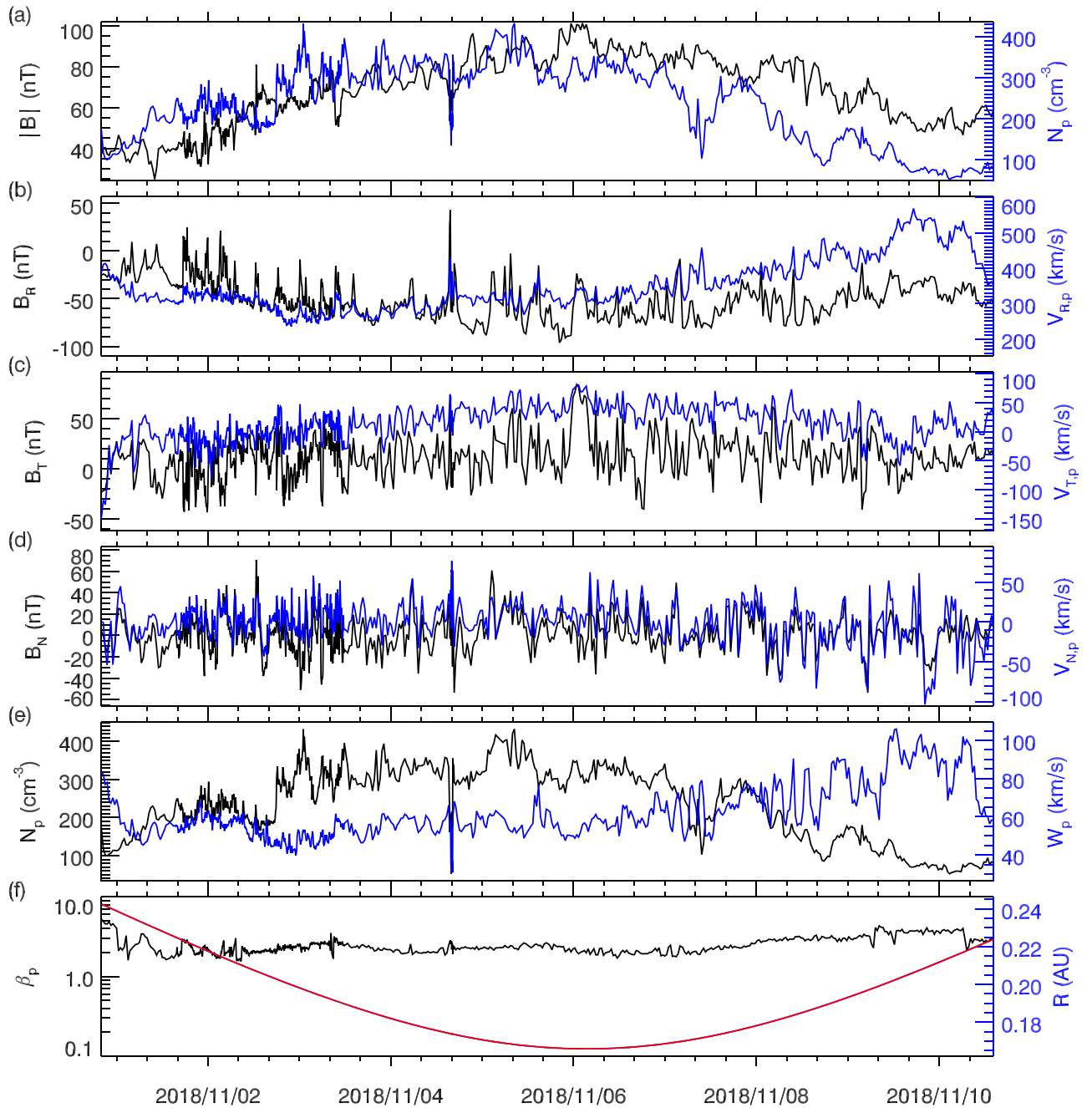
Figure 1. Time sequences overview of magnetic and plasma measurements during PSP's first encounter. Panel (a): magnetic field strength (|B|) and proton density (N_p). Panels (b), (c), and (d): magnetic fields (B_R, B_T, B_N) and proton bulk velocities ($V_{R,p}$, $V_{T,p}$, $V_{N,p}$) in RTN coordinates. Panel (e): proton density (N_p) and thermal velocity (W_p). Panel (f): plasma beta (β) and heliocentric distance (R) of spacecraft's position.

controversially discussed. There are many means to diagnose the wave modes: correlation analysis between velocity and magnetic field fluctuations (Wang et al. 2012; Šafránková et al. 2019), cross-helicity analysis (Roberts et al. 1987), comparison of the MHD dispersion relations derived from measurements with theory predictions (Shi et al. 2015), and mode-recognition methods (Glassmeier et al. 1995; Narita & Marsch 2015; Chaston et al. 2020). According to these studies, non-compressive outward Alfvén modes dominate the fluctuations in the solar wind especially in fast streams (Bruno & Carbone 2013). Compressive waves likely suffer strong Landau damping (Barnes 1966), resulting in their suppression in the overall fluctuations. Correlations among variables (e.g.,

magnetic pressure, thermal pressure, density, and temperature) show that the compressive component of magnetosonic waves and pressure-balanced structures exists simultaneously (PBSs; Kellogg & Horbury 2005; Yao et al. 2011; Yang et al. 2017). The majority of the compressive fluctuations is slow-mode-like rather than fast-mode-like in polarization (Howes et al. 2012; He et al. 2015; Shi et al. 2015). In situ observations show that the Alfvénicity decreases with heliocentric distance, which is potentially caused by the increased contribution of inward-propagating Alfvén waves or the compressive fluctuations (Bruno & Bavassano 1993).

To further comprehend the underlying multi-scale nature and evolution of near-Sun turbulence, we systematically study the
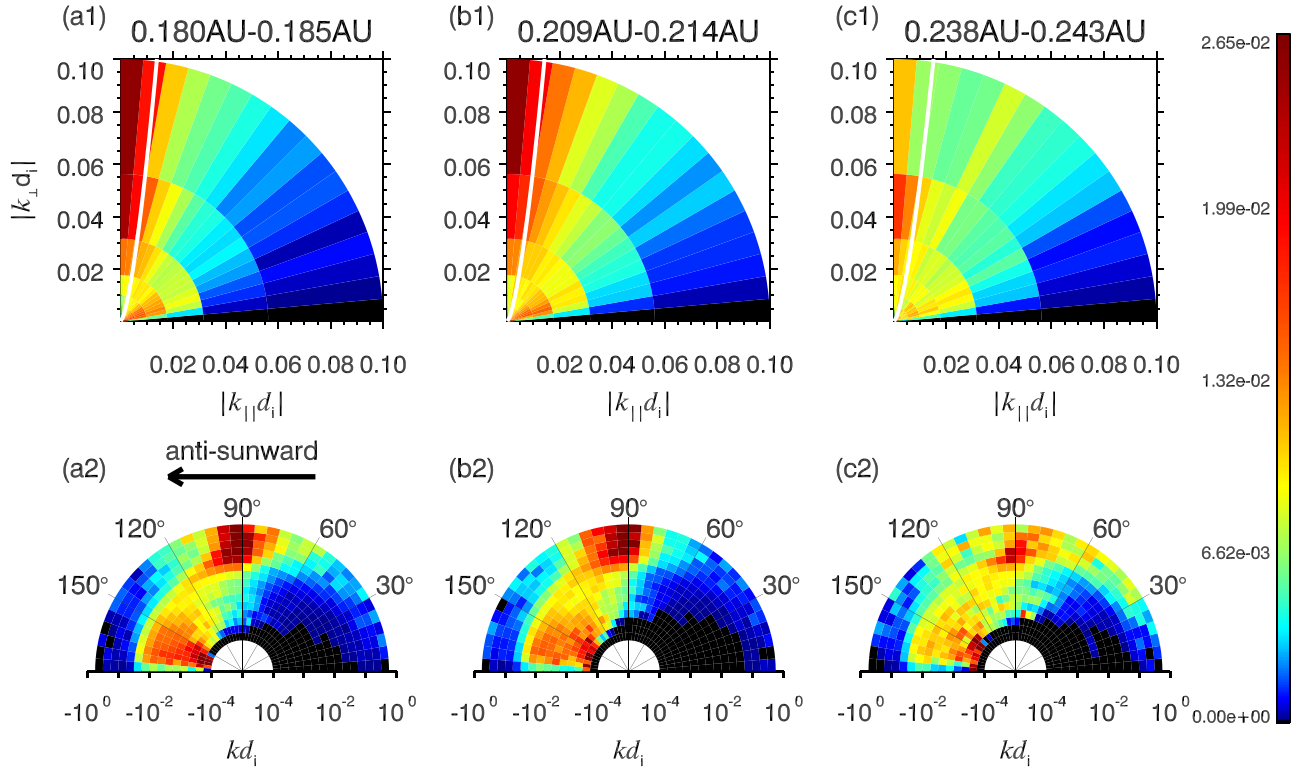
Figure 2. Panels (a1), (b1), and (c1): PDFs of the wavevector in $|k_\parallel d_i| - |k_\perp d_i|$ space in the range of 0.180 au–0.185 au, 0.209 au–0.214 au, and 0.238 au–0.243 au, respectively. The white solid lines represent the relation between $k_\parallel$ and $k_\perp$ as predicted from the phenomenology of critical balance, $k_\parallel \sim k_\perp^{\frac{2}{3}} k_0^{\frac{1}{3}}$, where k_0 is the wavenumber of the outer scale. Panels (a2), (b2), and (c2): PDFs of the propagation angle (θ_{k,B_0}) at differing scales (kd_i), in the corresponding distance ranges.

variation of the fluctuations' properties with scale and heliocentric distance within 0.3 au. The properties include the propagation direction of the wave, the mode composition, and the characteristic anisotropy on average. In Section 2, we briefly introduce the data sets that we use. In Section 3, we present our methods and analysis results, and give our summary and conclusions in Section 4. Our observations provide observational evidence for the verification of existing theoretical models at closer heliocentric distances, and also impose constraints on the improvement of existing theoretical models and the proposal of new models.

2. Data Sets and Data Deduction

We conduct our analysis using the data obtained from Parker Solar Probe (PSP), which is the closest human-built satellite to the Sun up to now (Fox et al. 2016). We use the Level-2 magnetic field data supplied by the Flux-gate Magnetometer (MAG; Bale et al. 2016) and the Level-3i proton data provided by the Solar Probe Cup (SPC; Kasper et al. 2016). The time interval investigated spans from UTC2018-10-31/20:00:00 to UTC2018-11-10/15:00:00 in which period PSP cruised between 0.166 au (35.78 solar radii) and 0.243 au (56.37 solar radii). The interval that we choose is shorter than the high-cadence interval around the first perihelion, because there are several sampling gaps longer than 30 minutes in the other intervals from which the SPC data are unavailable. We analyze time periods of the fluctuations in the range from 10 s to 1000 s, corresponding to MHD scales in the plasma frame. We do not exclude the so-called "switchback" patterns that exist among various scales (see Bale et al. 2019; Kasper et al. 2019; Dudok de Wit et al. 2020).

For the analysis of propagation direction and fluctuation anisotropy, we use the Singular Value Decomposition (SVD) method to resolve the frequencies and wavevectors of the waves based on Faraday's law. We estimate the three singular values of the spectral matrix (Equation (8) of Santolík et al. 2003), based on the principle of divergence-free magnetic field. We estimate the electric field at MHD scales for our SVD analysis as $E = -V_i \times B$ (Shi et al. 2015), where V_i is the proton bulk velocity obtained from SWEAP/SPC. We note that only one wavevector is solved for every specific frequency with the SVD method. Therefore, the resolved frequency and wavevector can be regarded as the frequency and wavevector of the major wave mode. In reality, it is possible that multiple wave modes exist in the turbulence at the same time and scale. For the mode composition analysis, we use the method suggested by Glassmeier et al. (1995), and obtain the contributions of the six MHD modes (parallel and anti-parallel propagating Alfvén mode, fast mode and slow mode) to the fluctuations. We estimate the spectral energy density of each mode as $e_i^T S(f_{sc}, t) e_i$, where $S(f_{sc}, t)$ is the spectral density matrix as defined by Glassmeier et al. (1995) and e_i is the eigenvector of the corresponding mode.

3. Analysis Results

We present an overview of the observed magnetic field and plasma measurements in Figure 1. To highlight the correlated fluctuations of the variables over such a long duration of about 10 days, we smooth all the measurements with a running window of 30 min. Figure 1(a) shows that the proton density (N_p) and the magnetic field strength ($|B|$) decrease with increasing heliocentric distance. The three components of the
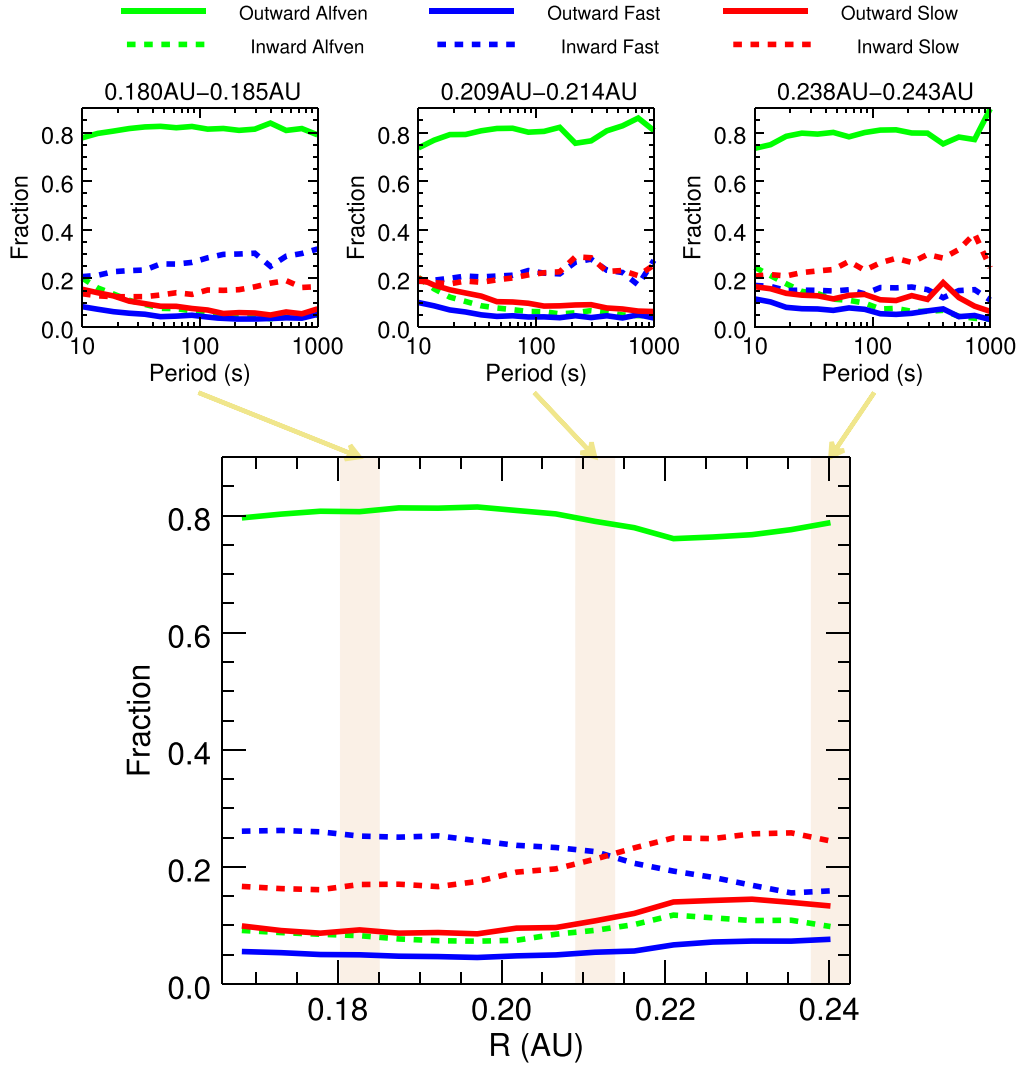
Figure 3. Top row: the period-dependent variation of the spectral fractions of the six MHD modes, i.e., outward/anti-sunward (solid line) and inward/sunward (dashed line) propagating Alfvén modes (green), fast modes (blue), and slow modes (red), as averaged over different distance ranges: 0.180 au–0.185 au (top-left panel), 0.209 au–0.214 au (top-middle panel) and 0.238 au-0.243 au (top-right panel), respectively. Bottom row: the heliocentric distance variation of the spectral fractions of the six MHD modes as averaged over the timescale (period) from 10 to 1000 s. The lime shadow sections correspond to the distance ranges used for the averaging of the intervals in the top row.

magnetic field (B_R, B_T, B_N) and the proton velocity ($V_{R,p}$, $V_{T,p}$, $V_{N,p}$) in RTN coordinates are positively correlated, respectively, which suggests that the large-scale outward-propagating Alfvénic fluctuations are dominant during this encounter. The proton thermal velocity (W_p) varies between $50 \, \mathrm{km \, s^{-1}}$ and $100 \, \mathrm{km \, s^{-1}}$ and there is no global correlation between the proton density and the thermal velocity. The plasma beta (β_p) is around 2, which does not exhibit a significant variation with heliocentric distance (R).

We solve the wavevector, $\boldsymbol{k}(\tau, R(t))$, at different heliocentric distances ($R(t)$) and periods (τ), where R is a function of time (t). The local background magnetic field, $\boldsymbol{B}_0(\tau, R(t))$, is acquired by Gaussian-weighting of the magnetic field time series at time t, where the width of the Gaussian profile is defined by the period τ (Podesta 2009). We then calculate the angles between $\boldsymbol{k}$ and $\boldsymbol{B}_0$, $\theta_{k,B_0}(\tau, R(t))$. Figure 2 (a1), (b1) and (c1) show the probability distribution functions (PDFs) of wavevectors in three distance ranges. For $kd_i > 0.02$, the wavevectors cluster around the quasi-perpendicular direction.

For $kd_i < 0.02$, the most probable wavevectors are quasi-parallel, relative to the local background magnetic field. Figure 2 (a2), (b2), and (c2) show the PDFs of θ_{k,B_0} depending on kd_i, in three different distance ranges. The propagation angles are close to 160° for $kd_i < 0.02$, and close to 90° for $kd_i < 0.02$. This indicates that the propagation angles are scale-dependent and turn from quasi-parallel at large scales to quasi-perpendicular at small scales.

We carry out a mode composition diagnosis (Glassmeier et al. 1995) and directly obtain the fractional contributions of the six MHD wave modes, at different heliocentric distances and periods. According to the radial component of the local background magnetic field, $B_{0r} = \boldsymbol{B}_0 \cdot \hat{\boldsymbol{e}}_r$, we transform the parallel and anti-parallel modes into outward/anti-sunward modes when $\boldsymbol{k} \cdot \boldsymbol{B}_0 > 0$, and inward/sunward modes when $\boldsymbol{k} \cdot \boldsymbol{B}_0 < 0$, respectively. The variation results of the averaged fractions of the transformed MHD modes are shown in Figure 3. The upper three panels show the variation of the fractions of the MHD modes with period averaged over the
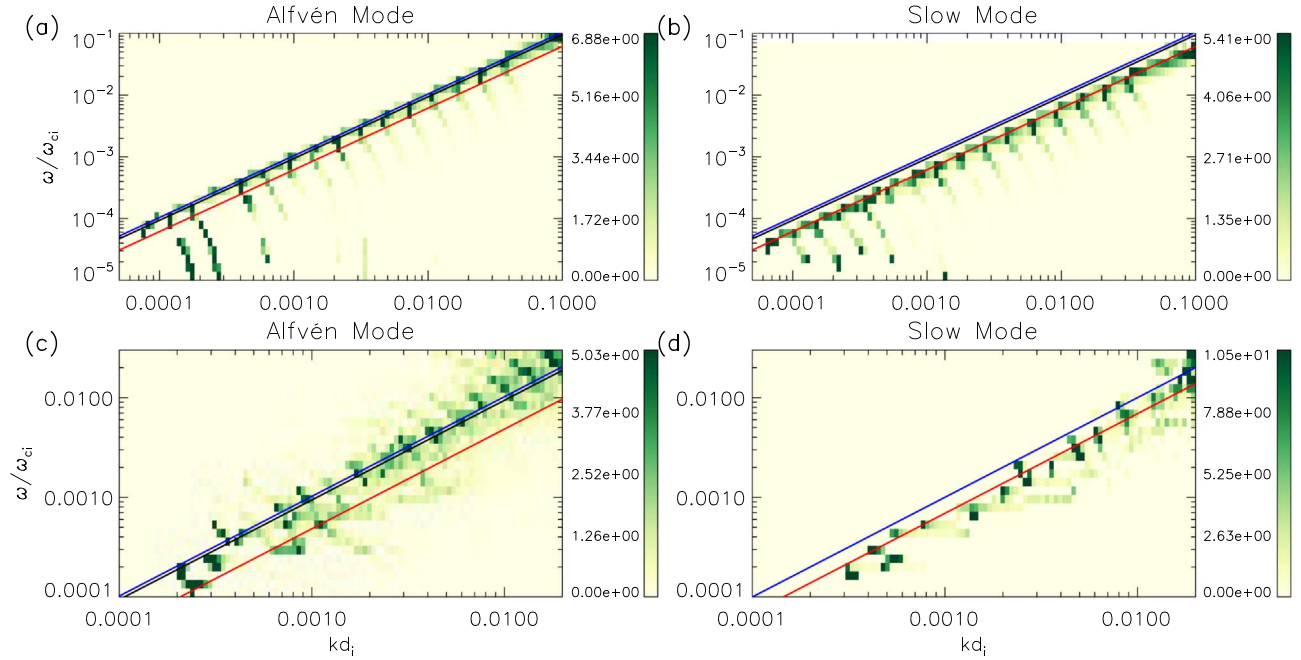
Figure 4. Panels (a) and (b): the PDFs of the normalized wavenumbers, kd_i, for Alfvén waves and slow waves, at each normalized angular frequency, ω/ω_{ci} in the plasma frame, resolved by a benchmark test of the SVD method, with MHD Alfvén-mode and MHD slow-mode fluctuations. The theoretical MHD dispersion relations of Alfvèn mode, fast mode and slow mode are plotted in black, blue, and red solid lines, respectively. Panels (c) and (d): the PDFs of kd_i for Alfvén waves and slow waves, at each ω/ω_{ci}, obtained from application of the SVD method to the magnetic and velocity measurements from PSP in [20:00, 21:00] UT on 2018 November 5 (panel (c)) and [18:20, 18:25] UT on 2018 November 4 (panel (d)), consistent with the dispersion relations of Alfvén and slow modes, respectively. Unlike in panels (a) and (b), we use the averaged plasma parameters over the corresponding time intervals in panels (c) and (d).

distance ranges of 0.180 au–0.185 au, 0.209 au–0.214 au, and 0.238 au–0.243 au, respectively. The wave mode occupying the highest spectral proportion is the outward Alfvén mode at most scales in these three R-intervals. The outward fast mode, the inward Alfvén mode, and the outward slow mode represent the modes with the lowest fractional proportions throughout the whole MHD range at these distances. The fractional proportions of these three modes slightly increase with increasing distance. On average, from 0.180 au to 0.185 au, the inward fast mode is the second-most abundant mode, while the inward slow mode is in third place. From 0.209 au to 0.214 au, the inward slow mode and the inward fast mode have approximately equal proportions. From 0.238 au to 0.243 au, the inward slow mode is in second place, followed by the inward fast mode. We also find this change of mode composition with distance in the radial variation of the period-averaged fraction of mode compositions (see the bottom panel of Figure 3). The outward Alfvén mode dominates throughout the whole near-Sun region under investigation. The fractional contribution of the fast mode decreases with increasing distance, while the contribution from inward slow modes increase with distance.

To further verify this composition diagnosis results, we reconstruct the dispersion relations of Alfvén waves and slow waves, as shown in Figure 4. We first demonstrate a benchmark test to verify the ability of the SVD method to resolve the MHD dispersion relations. The preset basic parameters are: bulk velocity, $V_0 = 400$ km s^{-1}, background magnetic field, $B_0 = 90$ nT, proton number density, $n_p = 300$ cm^{-3}, proton thermal velocity, 60 km s^{-1}, and $\theta_{k,B_0} = 20°$. Based on the polarization relations of the Alfvén mode and slow mode, we set up the corresponding magnetic field and velocity disturbances of the two modes, and use these disturbances as an artificial data input

of the SVD method. In order to test the robustness of the SVD method, we also add noise at the level of 0.1% for each wave at all scales to the virtual data input. As a result, we obtain a solution in terms of the wavevector (kd_i) at every frequency (ω/ω_{ci}) and during every local time interval, where ω_{ci} is the ion-cyclotron frequency. Furthermore, we construct the PDF (kd_i, ω/ω_{ci}) statistically based on the information of $kd_i(\omega/\omega_{ci}, t)$. The PDFs ($kd_i$, ω/ω_{ci}) for the benchmark tests of the Alfvén mode and slow mode are illustrated in Figure 4(a) and 4(b). The dispersion relations as indicated by the ridges with high PDF values are fully consistent with the theoretical dispersion relations, which means that the SVD method is well able to resolve the MHD dispersion relations from our observations. Hereafter, we apply the SVD method to the observational measurements to examine whether the dispersion relations of Alfvén waves and slow waves prevail. The results are shown in Figure 4(c) and Figure 4(d). The green patches corresponding to high levels of PDF concentrate on and around the theoretical dispersion relations of MHD Alfvén and slow modes. These results further confirm the existence of incompressible Alfvén waves (the most prevalent component) and compressible slow waves (the sub-dominant component).

Lastly, we investigate the variation of the fluctuation anisotropy with period and distance in Figure 5. The ratio of the middle and maximum singular values of the spectral matrix (Equation (8) of Santolík et al. 2003), $\lambda_{mid}/\lambda_{max}$, is adopted to represent the anisotropy of the magnetic field fluctuations in the plane perpendicular to the propagation direction, which we take to be oriented along the direction with the minimum singular value λ_{min}. $\lambda_{mid}/\lambda_{max}$ is also known as the ellipticity. The ratio increases from around 0.3 to over 0.37 as the wave period increases, throughout the distance range under investigation.
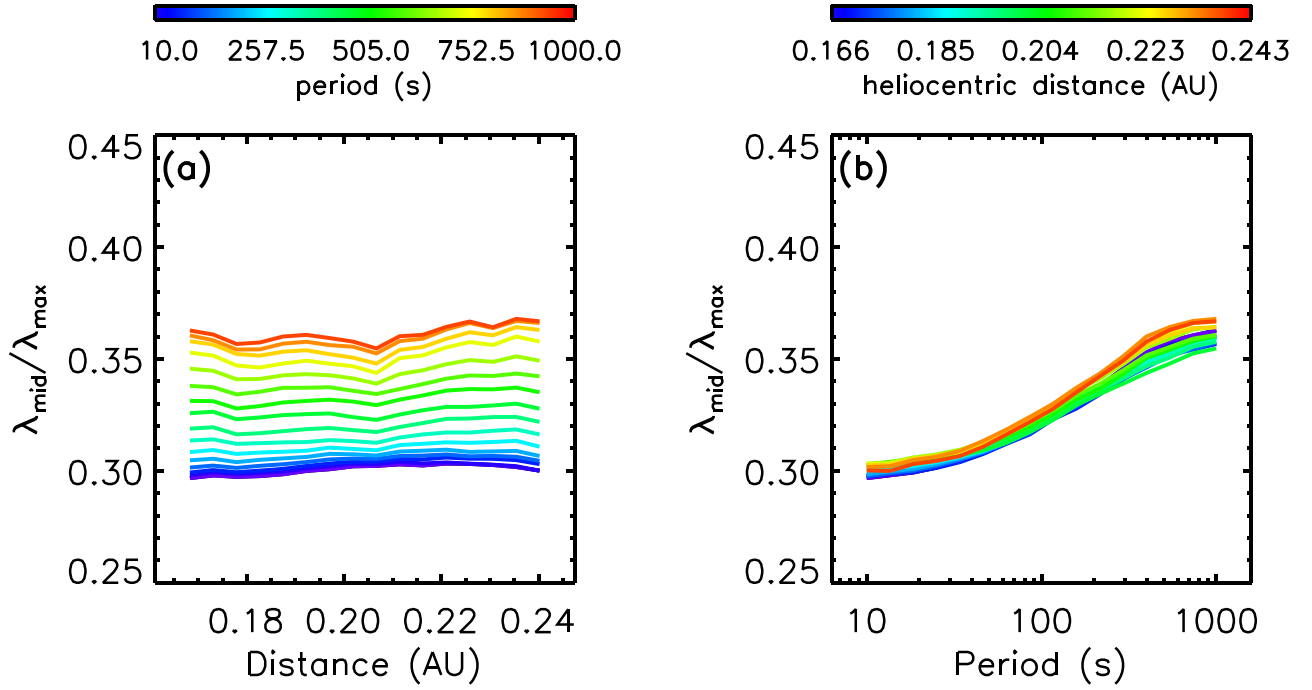
Figure 5. Panel (a): the distance profiles of the ratio between the middle and maximum singular values of the magnetic spectral matrix ($\lambda_{mid}/\lambda_{max}$) for the magnetic fluctuations at different periods from 10 to 1000 s. Panel (b): the variations of $\lambda_{mid}/\lambda_{max}$ with period for the magnetic fluctuations at different distances from 0.17 to 0.24 au.

According to the above analysis, the dominant Alfvén mode increases in its degree of circular or arc polarization with increasing period.

4. Conclusion

The diversity, complexity, and evolution of solar wind turbulence have always been important research topics in heliospheric physics. Hence, we statistically study mode propagation, mode composition, and fluctuation anisotropy of the solar wind MHD turbulence as measured by PSP. We find the following.

(1) At 0.166 au $< R <$ 0.243 au, the propagation angles (θ_{k,B_0}) of wave-like turbulent fluctuations for $kd_i < 0.02$ are greater than 135°, mainly concentrating around 160°, while the distribution gradually shifts its center to $\theta_{k,B_0} \sim 90°$ for $0.02 < kd_i < 0.1$.

(2) The distance variations of the scale-averaged fractions of the MHD modes show that: (a) the outward/anti-sunward propagating Alfvén mode dominates the mode composition throughout the whole investigated range of distances, while the outward slow mode, the inward/sunward Alfvén mode and the outward fast mode represent the three smallest proportions; (b) the fraction of the inward fast mode decreases with distance, whereas the fraction of the inward slow mode increases with distance; (c) at 0.166 au $< R <$ 0.215 au, the inward fast mode takes the second place and the inward slow mode is in third place; at 0.215 au $< R >$ 0.243 au, the inward slow mode is in third place followed by the inward fast mode.

(3) The ellipticity increases with spacecraft-frame period in the heliocentric distance range studied.

According to the critical-balance hypothesis (Goldreich & Sridhar 1995; Horbury et al. 2008), the anisotropy of the power

spectrum follows from the condition that the nonlinear time and the propagation time are approximately equal ($k_{\parallel}V_A \sim k_{\perp}\delta v$) in strong MHD turbulence with balanced Elsässer fluxes. However, in solar wind turbulence with imbalanced fluxes dominated by outward Alfvén waves, our PDF of wave propagation in $k_{\parallel}-k_{\perp}$ space (see color maps in Figure 2) is inconsistent with this prediction of critical-balance theory (see the white solid lines in Figure 2). For $kd_i < 0.02$, the most probable wavevector is more parallel, while for $kd_i > 0.02$, the most probable wavevector is closer to the quasi-perpendicular direction. This observational result will help to enlighten and promote the theory of turbulence anisotropy characterized by a transition of propagation direction from quasi-parallel to quasi-perpendicular with a large angular jump at a certain scale. After integrating the ideas of both "slab+2D" and "critical-balance" scenarios, an upgraded turbulence phenomenology in Fourier space was proposed to involve "quasi-parallel wavelike fluctuations" and "quasi-2D fluctuations" as well as energy transfer between them and within themselves (Oughton et al. 2015). The observed transition from quasi-parallel to quasi-perpendicular propagation with increasing wavenumber shows a way to improve turbulence models in the future.

The transition of the dominant outward Alfvén mode from $\theta_{k,B_0} \sim 160°$ to $\theta_{k,B_0} \sim 90°$, as the period decreases from 1000 s to 10 s, may also indicate the geometry of the Alfvén waves at kinetic scales in the near-Sun solar wind. Quasi-perpendicular Alfvén waves are more likely to dominate at scales closer to the ion scale. Accordingly, quasi-perpendicular modes (e.g., kinetic Alfvén waves) may participate in the turbulent cascade and further dissipation, energizing and shaping nonthermal ion distributions, which may develop temperature anisotropy and feed back to excite the ion-cyclotron waves reported during this interval (Bowen et al. 2020). In the future, we will study the following chain of energy conversion processes: damping of

quasi-perpendicular kinetic waves $\longrightarrow$ energization of particles $\longrightarrow$ growth of quasi-parallel waves.

In some respect, our mode composition diagnosis results differ from the results of Chaston et al. (2020). They study the spectral energy density fractions of six MHD modes inside and outside the field reversal regions, separately. They report that the three outward (anti-sunward) modes are dominant at MHD scales on average. This difference may lie in the calculation of the propagation angle, which is an input parameter of the mode-recognition method (Glassmeier et al. 1995). Chaston et al. (2020) obtained the propagation direction using the spectral matrix of the magnetic field only as suggested by Samson & Olson (1980), while we use both the magnetic and the electric field based on the Faraday's law (Santolík et al. 2003). This aspect may lead to the different results regarding the mode composition.

The ellipticity serves here as an indicator to distinguish if the polarization is circular ($\lambda_{\mathrm{mid}}/\lambda_{\mathrm{max}} \sim 1$), arc ($0 < \lambda_{\mathrm{mid}}/\lambda_{\mathrm{max}} < 1$), or linear ($\lambda_{\mathrm{mid}}/\lambda_{\mathrm{max}} \sim 0$). The ellipticity increases with the period of the fluctuations from 0.3 to 0.37, which indicates that the magnetic fluctuations tend to be more and more circular-polarized as the period increases. Based on Figure 2, the waves are also quasi-parallel propagating at greater periods. This observation is consistent with the prediction that the Alfvén branch of the MHD solutions is circular-polarized when $\theta_{\mathrm{k,B_0}} \sim 0°$.

ORCID iDs

Xingyu Zhu ⓘ https://orcid.org/0000-0002-1541-6397
Jiansen He ⓘ https://orcid.org/0000-0001-8179-417X
Daniel Verscharen ⓘ https://orcid.org/0000-0002-0497-1096
Die Duan ⓘ https://orcid.org/0000-0002-6300-6800
Stuart D. Bale ⓘ https://orcid.org/0000-0002-1989-3596

References

Bale, S. D., Badman, S. T., Bonnell, J. W., et al. 2019, Natur, 576, 237
Bale, S. D., Goetz, K., Harvey, P. R., et al. 2016, SSRv, 204, 49
Bandyopadhyay, R., Matthaeus, W. H., Parashar, T. N., et al. 2020, ApJS, 246, 61
Barnes, A. 1966, PhFl, 9, 1483
Bavassano, B., Dobrowolny, M., Fanfoni, G., Mariani, F., & Ness, N. F. 1982, SoPh, 78, 373
Bowen, T. A., Mallet, A., Huang, J., et al. 2020, ApJS, 246, 66
Bruno, R., & Bavassano, B. 1993, P&SS, 41, 677
Bruno, R., & Carbone, V. 2013, LRSP, 10, 2
Chaston, C. C., Bonnell, J. W., Bale, S. D., et al. 2020, ApJS, 246, 71
Chen, C. H. K., Bale, S. D., Bonnell, J. W., et al. 2020, ApJS, 246, 53
Chhiber, R., Goldstein, M. L., Maruca, B. A., et al. 2020, ApJS, 246, 31
Coleman, Paul J., Jr. 1966, JGR, 71, 5509
Cranmer, S. R., & Winebarger, A. R. 2019, ARA&A, 57, 157
D'Amicis, R., & Bruno, R. 2015, ApJ, 805, 84
Dobrowolny, M., Mangeney, A., & Veltri, P. 1980, PhRvL, 45, 144
Duan, D., Bowen, T. A., Chen, C. H. K., et al. 2020, ApJS, 246, 55
Dudok de Wit, T., Krasnoselskikh, V. V., Bale, S. D., et al. 2020, ApJS, 246, 39
Fox, N. J., Velli, M. C., Bale, S. D., et al. 2016, SSRv, 204, 7
Glassmeier, K. H., Motschmann, U., & von Stein, R. 1995, AnGeo, 13, 76
Goldreich, P., & Sridhar, S. 1995, ApJ, 438, 763
He, J., Tu, C., Marsch, E., et al. 2015, ApJL, 813, L30
He, J., Tu, C., Marsch, E., Bourouaine, S., & Pei, Z. 2013, ApJ, 773, 72
He, J. S., Tu, C. Y., & Marsch, E. 2007, A&A, 468, 307
Horbury, T. S., Forman, M., & Oughton, S. 2008, PhRvL, 101, 175005
Horbury, T. S., Matteini, L., & Stansby, D. 2018, MNRAS, 478, 1980
Howes, G. G., Bale, S. D., Klein, K. G., et al. 2012, ApJL, 753, L19
Kasper, J. C., Abiad, R., Austin, G., et al. 2016, SSRv, 204, 131
Kasper, J. C., Bale, S. D., Belcher, J. W., et al. 2019, Natur, 576, 228
Kellogg, P. J., & Horbury, T. S. 2005, AnGeo, 23, 3765
Matteini, L., Horbury, T. S., Neugebauer, M., & Goldstein, B. E. 2014, GeoRL, 41, 259
Narita, Y., & Marsch, E. 2015, ApJ, 805, 24
Oughton, S., Matthaeus, W. H., Wan, M., & Osman, K. T. 2015, RSPTA, 373, 20140152
Parashar, T. N., Goldstein, M. L., Maruca, B. A., et al. 2020, ApJS, 246, 58
Parker, E. N. 1958, ApJ, 128, 664
Perrone, D., D'Amicis, R., De Marco, R., et al. 2020, A&A, 633, A166
Perrone, D., Stansby, D., Horbury, T. S., & Matteini, L. 2019, MNRAS, 483, 3730
Podesta, J. J. 2009, ApJ, 698, 986
Qudsi, R. A., Maruca, B. A., Matthaeus, W. H., et al. 2020, ApJS, 246, 46
Roberts, D. A., Klein, L. W., Goldstein, M. L., & Matthaeus, W. H. 1987, JGR, 92, 11021
Samson, J. C., & Olson, J. V. 1980, GeoJ, 61, 115
Santolík, O., Parrot, M., & Lefeuvre, F. 2003, RaSc, 38, 1010
Shi, M. J., XIAO, C. J., LI, Q. S., et al. 2015, ApJ, 815, 122
Šafránková, J., Němeček, Z., Němec, F., et al. 2019, ApJ, 870, 40
Stansby, D., & Horbury, T. S. 2018, A&A, 613, A62
Tu, C., & Marsch, E. 1995, SSRv, 73, 1
Tu, C. Y., Marsch, E., & Thieme, K. M. 1989, JGR, 94, 11739
Tu, C.-Y., Zhou, C., Marsch, E., et al. 2005, Sci, 308, 519
Wang, X., He, J., Tu, C., et al. 2012, ApJ, 746, 147
Wang, X., Zhao, L., Tu, C., & He, J. 2019, ApJ, 871, 204
Yang, L., Zhang, L., He, J., et al. 2017, ApJ, 851, 121
Yao, S., He, J. S., Marsch, E., et al. 2011, ApJ, 728, 146